PAPER

Check for updates

Noble metal sensitized invasive porous bioelectrodes: advanced medical device for enhanced neuronal activity and chronic alcohol treatment†

Hong Soo Kim, [ID] ‡[a] Hansaem Choi,‡[a] Monica Claire Flores,‡[a] Abdul Razzaq,[b] Young Seob Gwak,[c] Danbi Ahn,[c] Mi Seon Kim,[d] Ogan Gurel,[e] Bong Hyo Lee*[f] and Su-Il In [ID] *[a]

Invasive bioelectrodes are widely used as an effective treatment for several acute and chronic diseases. In earlier work using high surface area invasive porous bioelectrodes evaluated in an animal model of alcoholism withdrawal, we demonstrated significantly improved electrophysiological and behavioral responses. In this study, we further modify the surface of these invasive porous bioelectrodes with noble metal (Ag, Au, Pt) nanoparticles. Compared to both conventional and porous bioelectrodes, noble metal sensitized invasive porous bioelectrodes show markedly increased low threshold (LT) and wide dynamic range (WDR) neuronal activity. In particular, Pt-sensitized invasive porous bioelectrodes show the highest WDR neuronal activity only upon insertion. In addition, Ag-sensitized invasive porous bioelectrodes, whose surface area is about 37 times greater than that of conventional bioelectrodes, show improved electrochemical properties with higher LT and WDR neuronal activity when stimulated. In an animal model of chronic alcoholism, using normal and alcohol-treated Sprague-Dawley (SD) rats evaluated with the elevated plus maze (EPM) test, the Ag-sensitized invasive porous bioelectrodes show about 20% higher open arms time. These results suggest that these noble metal-sensitized invasive bioelectrodes may offer improved therapeutic outcomes for the treatment of chronic alcoholism, and given these enhanced electrophysiological properties, for other conditions as well.

1. Introduction

The use of invasive bioelectrodes has long been accepted as an effective treatment modality for a variety of conditions, including intractable pain,[1] drug addiction,[2] psychiatric

[a]Department of Energy Science & Engineering, Daegu Gyeongbuk Institute of Science & Technology (DGIST), 333 Techno Jungang-daero, Hyeonpung-eup, Dalseong-gun, Daegu, 42988, Republic of Korea. E-mail: insuil@dgist.ac.kr

[b]Department of Chemical Engineering, COMSATS University Islamabad, Lahore Campus, 1.5 km Defence Road, Off Raiwind Road, Lahore, 54000, Pakistan

[c]Department of Physiology, College of Korean Medicine, Daegu Haany University, 136 Sincheondong-ro, Suseong-gu, Daegu, 42158, Republic of Korea

[d]Clinical Trials Management Division, Pharmaceutical Safety Bureau, Ministry of Food and Drug Safety, Cheongju-si, Chungcheongbuk-do, Republic of Korea

[e]College of Transdisciplinary Studies, Daegu Gyeongbuk Institute of Science & Technology (DGIST), 333 Techno Jungang-daero, Hyeonpung-eup, Dalseong-gun, Daegu, 42988, Republic of Korea

[f]Department of Acupuncture, Moxibustion, and Acupoint, College of Korean Medicine, Daegu Haany University, 136 Sincheondong-ro, Suseong-gu, Daegu, 42158, Republic of Korea. E-mail: dlqhdgy@dhu.ac.kr

† Electronic supplementary information (ESI) available. See DOI: 10.1039/d0ra07922g

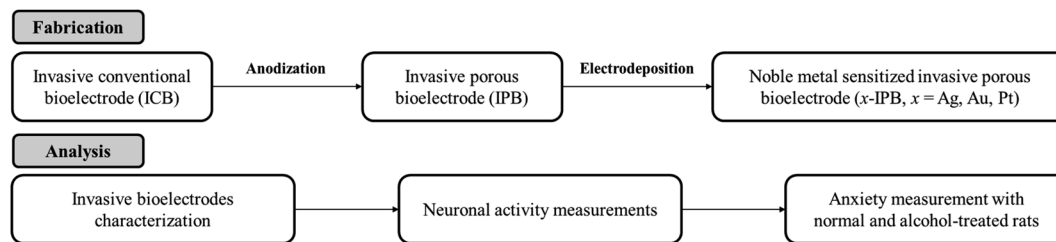‡ These authors contributed equally to this work.

disorders,[3] stroke rehabilitation,[4] headaches,[5] myofascial pain,[6] osteoarthritis,[7] and back pain.[8] Historically, materials of invasive bioelectrodes have varied from ceramic to noble metal.[9] Modern invasive bioelectrodes are generally fabricated from stainless steel[9–11] because of their relatively low cost, ease of fabrication, and high biocompatibility,[12] thus are inserted at specific points in the body for treatment.[13] While the underlying biological mechanism of invasive bioelectrode treatment remains as yet undetermined, it has been largely accepted that the inserted bioelectrode interacts mechanically and electrochemically with the surrounding tissue, thus altering the neurochemical balance of the peripheral and central nervous systems.[14–19]

Several approaches have been investigated for enhancing the efficacy of invasive bioelectrode treatment, including variations in the diameter,[20] insertion depth,[21,22] and a number of bioelectrodes employed during treatment.[23] Another strategy has been used to modify the bioelectrode surface, for example, with graphene, an excellent electrical conductor, or with noble metals.[24,25] Oriental medicine practitioners have also tried a variety of procedural variations, such as lifting-thrusting or twisting-rotating manipulations to further improve invasive

Fig. 1 Schematic illustration of whole experimental procedures.

bioelectrode treatment.[26,27] These enhanced manipulations are believed to improve results by promoting various neuronal, biophysical, and biochemical reactions,[28] although such stimulation methods may cause undesirable effects in the patient, such as feelings of fullness, numbness, soreness, heaviness, pressure, as well as tingling.[29–31]

In previous studies, we fabricated invasive porous bioelectrodes with a high surface area and low electrochemical resistance *via* electrochemical anodization, resulting in increased invasive bioelectrode therapeutic efficacy. Application of these modified invasive bioelectrodes showed improved therapeutic properties as well as enhanced therapeutic treatment of colorectal cancer.[32–35] Surface modification of invasive bioelectrodes with noble metal nanoparticles has recently attracted considerable interest due to their distinct electrical, plasmonic, and electrocatalytic properties.[36–39] Noble metal modified invasive bioelectrodes have been considered for neural stimulation,[36] modulation of neuronal behavior,[37] neurotransmitter detection,[38] and intrinsic therapeutic measurements.[39]

In this study, we first report, to the best of our knowledge, the novel development of invasive porous bioelectrodes sensitized with noble metal nanoparticles, as well as the detailed characterization of their electrophysiological effects on neuronal activity and their use in treating chronic alcoholism. Fig. 1 represents the schematic illustration and tactic of the whole study. The fabrication strategy involves the electrochemical anodization of an invasive conventional bioelectrode (ICB), as reported previously,[32] resulting in an invasive porous bioelectrode (IPB) with a very high surface area, followed by electrodeposition of three different noble metal nanoparticles, *i.e.*, silver (Ag), gold (Au) or platinum (Pt), generating the metal sensitized porous bioelectrodes (x-IPB, where x represents the specific noble metal used). Fig. S1 in the ESI† illustrates this sequential fabrication of a noble metal nanoparticle sensitized invasive porous bioelectrode. Using an *in vivo* Sprague-Dawley rat model, we find the noble metal sensitized porous bioelectrodes, compared to conventional bioelectrodes as well as unsensitized invasive porous bioelectrodes, exhibit significantly improved electrophysiological neuronal activity. In particular, silver nanoparticle sensitized invasive porous bioelectrodes (Ag-IPB) show high alcohol detoxification with bioelectrode stimulation. We believe this to be the first report of noble metal sensitized invasive porous bioelectrodes showing enhanced neuronal activity and a substantial alcohol detoxification effect.

2. Results and discussion

2.1. Invasive bioelectrode characterization

Fig. 2a–e shows Field Emission Scanning Electron Microscope (FE-SEM) surface images of an invasive conventional bioelectrode (ICB), an invasive porous bioelectrode (IPB), and noble metal nanoparticle sensitized invasive porous bioelectrodes (x-IPB) upon which nanoparticles of different noble metals (represented by x, where x = Ag, Au, Pt) have been
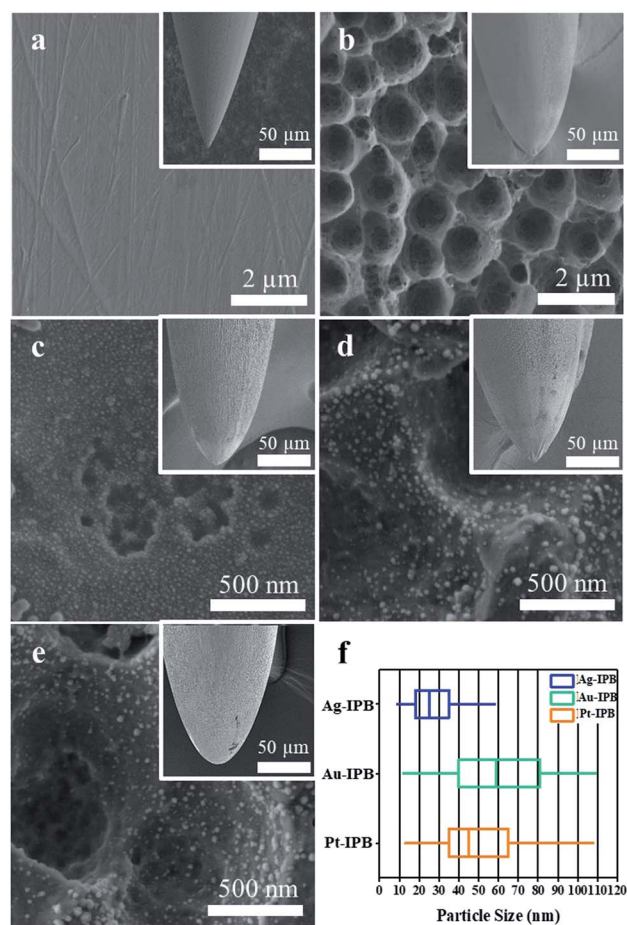

Fig. 2 FE-SEM surface images of: (a) invasive conventional bioelectrode (ICB), (b) invasive porous bioelectrode (IPB), (c) Ag-IPB, (d) Au-IPB and (e) Pt-IPB. The insert shows close up views of the bioelectrode tips. (f) Box plot showing median size values of electrodeposited nanoparticles.
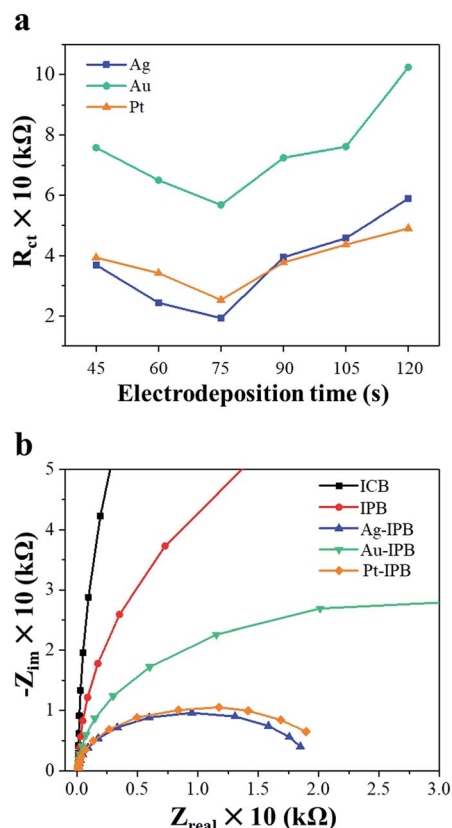
a

b

Fig. 3 (a) Charge transfer resistance (R_{CT}) vs. electrodeposition time for x-IPB of various electrodeposition times. (b) Fitted Nyquist plots corresponding to electrochemical impedance spectra (EIS) for ICB, IPB and x-IPB (2.0 V, 75 s electrodeposition).

electrodeposited. A box plot showing the median value (central line), with edges representing the 25th and 75th percentiles, is shown in Fig. 2f, illustrating the size variation of the nanoparticles.

Fig. S2 in the ESI† shows a high-resolution FE-SEM image of an IPB surface, from which the conical topology can be clearly seen; the pore depth appears from 0.3 to 0.8 μm, with an average pore diameter of 1.86 μm. Utilizing Image-J software the average size estimated for the Ag, Au and Pt nanoparticles are found to be 32.9, 57.7 and 49.3 nm, respectively (Fig. S3a–c in the ESI†). Fig. S4 in the ESI† shows FE-SEM images of noble metal nanoparticles electrodeposited upon invasive conventional bioelectrodes.

Fig. 3a shows the charge transfer resistance (R_{CT}), obtained by electrochemical impedance spectroscopy (EIS), of different x-IPB samples with different electrodeposition times. Among all samples those x-IPB specimens (x = Ag, Au, Pt) with an electrodeposition time of 75 s exhibited the lowest charge transfer resistance. Based on this result, an electrodeposition time of 75 s with applied voltage of 2.0 V was selected as the optimum condition for x-IPB fabrication. Fig. 3b shows the fitted Nyquist plots for ICB, IPB and x-IPB samples (75 s electrodeposition).

Elemental composition and surface areas before/after electrodeposition were determined using energy dispersive spectroscopy (EDS) and UV-Vis absorption spectra (Table 1). The elemental analysis indicates no significant variation in stainless steel bioelectrode composition after electrochemical anodization and nanoparticle deposition. Bioelectrode surface areas were determined using Methylene Blue (MB) dye adsorption employing Beer-Lambert's law.[40] Fig. S5 in the ESI† shows the UV-Vis absorption spectra for ICB, IPB, and x-IPB as a function of electrodeposition time. In comparison to ICB and IPB, all x-IPB samples show increased surface area, with increased electrodeposition time (Table S1 in the ESI†).

2.2. Neuronal activity measurements

x-IPB efficacy was evaluated by measurement of electrophysiological neuronal activity in response to bioelectrode stimulation. Before the electrophysiological tests, the basal mechanical sensitivity of each bioelectrode group was determined by measuring paw withdrawal thresholds (PWTs) to avoid differential sensitivity to mechanical stimulation (Fig. S6 in the ESI†). The average PWTs of the conventional (ICB) group is 15.23 ± 0.35 g and lies within the normal PWT range of rats.[41] The average PWTs of the porous bioelectrode (IPB) and metal-sensitized porous bioelectrodes (Ag-IPB, Au-IPB, and Pt-IPB) are determined to be 15.65 ± 0.53 g, 15.55 ± 0.47 g, 15.34 ± 0.57 g, and 15.81 ± 0.48 g, respectively, indicating that measurement of the bioelectrode stimulation-induced changes of spinal dorsal horn neuronal responses was performed without significant differences to mechanical sensitivity among all groups (Fig. S7 in the ESI†).

Changes in neuronal activity were measured for all invasive bioelectrodes (Fig. S8–S12 in the ESI†). The ICB group shows a significant improvement in low threshold (LT) neuron activity but no significant enhancement in wide dynamic range (WDR) neurons before and after bioelectrode stimulation (Fig. S8 in the

Table 1 Elemental analysis and surface areas before and after electrodeposition of noble metal nanoparticles (ICB, IPB and x-IPB), 2.0 V and 75 s electrodeposition time.

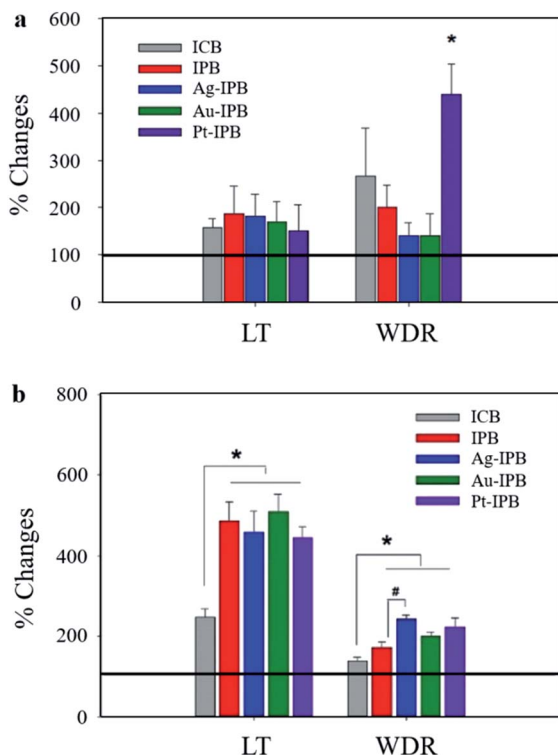| Elements	ICB Atom. C (at. %)	IPB Atom. C (at. %)	Ag-IPB Atom. C (at. %)	Au-IPB Atom. C (at. %)	Pt-IPB Atom. C (at. %)
x-Metal	—	—	0.29 ± 0.05	0.28 ± 0.07	0.23 ± 0.06
Fe	73.12 ± 1.14	70.36 ± 6.14	69.52 ± 1.57	63.42 ± 1.97	68.87 ± 2.13
Cr	17.87 ± 2.01	18.69 ± 1.71	17.87 ± 0.35	16.8 ± 0.56	16.37 ± 0.45
Ni	7.86 ± 2.11	8.01 ± 1.04	7.57 ± 0.22	7.30 ± 0.25	7.38 ± 0.18
Surface area ($m^2 g^{-1}$)	0.04	1.03	1.49	1.18	1.30

Fig. 4 Comparison of neuronal response activity. Changes of LT and WDR neuronal response (a) without bioelectrode stimulation, and (b) with bioelectrode stimulation in each group. Horizontal line: 100% of activity induced by VFFs stimulation.

ESI†). However, the unconventional bioelectrodes, including IPB and x-IPB (Ag-IPB, Au-IPB, and Pt-IPB, 2.0 V, 75 s) displayed significant enhancement in both LT and WDR neuronal responses, before and after bioelectrode stimulation (Fig. S9–S12 in the ESI†).

Fig. 4 shows the relative changes in neuronal activities. In particular, the activity of the Pt-IPB group in WDR neurons is $438.9 \pm 64.5\%$ and showed a significant increase ($*p < 0.05$) as compared to before stimulation, whereas other groups did not show any significant change. Fig. 4b shows changes in LT and WDR neuronal activities with bioelectrode stimulation: for ICB, the LT neuronal response is $247 \pm 20.8\%$, while the IPB, Ag-IPB, Au-IPB and Pt-IPB groups show markedly increased values of $487.3 \pm 46.7\%$, $459.5 \pm 52.7\%$, $510 \pm 44.2\%$ and $445.5 \pm 28\%$ ($*p < 0.05$), respectively. Regarding the WDR neurons, the neuronal responsiveness of ICB is $137.9 \pm 9.3\%$, whereas, IPB, Ag-IPB, Au-IPB and Pt-IPB groups show generally higher values of $170.9 \pm 14.3\%$, $242.2 \pm 9.8\%$, $199.3 \pm 9.7\%$ and $221.2 \pm 24.2\%$ ($*p < 0.05$), respectively.

2.3. Anxiety measurements with normal and alcohol-treated rats

Sprague-Dawley (SD) rats were evaluated with the elevated plus maze (EPM) test for anxiety both in the normal (non-alcohol-treated) and control (alcohol-treated) cases. The percentage of time in the open arms spaces, as compared to the enclosed

arms, is a well-established marker of anxiety. Fig. 5 shows the open arms time (as a percentage of the entire time) during withdrawal from chronic alcohol for each group. These results clearly show that the alcohol-treated (control) rats demonstrated much lower open arms time (higher anxiety) than the normal (untreated) animals. While treatment with all invasive bioelectrodes showed significantly increased open arms time (reduced anxiety in the context of alcohol withdrawal) as compared to the control group, the Ag-sensitized invasive porous bioelectrodes showed a statistically significant 20% higher open arms time as compared to rats treated with conventional and porous bioelectrodes.

2.4. Discussion

The ICB exhibits a uniformly smooth surface (Fig. 2a) while the IPB surface displays a hierarchical micro/nanoscale porous topology (Fig. 2b). As shown in Fig. 2c–e, the electrodeposition of noble metals resulted in a uniform loading of noble metal nanoparticles of less than 100 nm size on the surface of the porous bioelectrode. In addition, as the noble metal nanoparticles were uniformly electrodeposited on the IPB surface, the surface area of these x-IPB was further increased beyond that of the surface areas of the ICB and IPB. In particular, Ag-IPB showed the highest surface area ($1.49 \text{ m}^2 \text{ g}^{-1}$), which was about 37 times higher than ICB (Table 1). The same noble metal deposition method was also applied directly to the ICB, but this was found to be suboptimal due to lower surface area leading to aggregation of these nanoparticles (Fig. S4 in the ESI†).

In electrochemical properties, the noble metal invasive porous bioelectrodes fabricated in optimal conditions have lower electron transfer resistance (Fig. 3a) and electrochemical impedance (Fig. 3b) as compared to ICB and IPB. This suggests that maximum amounts of noble metal nanoparticles distributed on the surface of porous bioelectrode facilitate the transport of electrons. In addition, these nanoparticles provide a high surface area to volume ratio that increases the electrical conductivity and catalytic activity[42,43] of x-IPB. Therefore, the strategy of depositing noble metal nanoparticles on invasive porous bioelectrodes significantly increased the electrode surface area and improved its conductivity and electrochemical properties.

Based on the excellent properties of these noble metal sensitized invasive porous bioelectrodes, the neuronal activity according to the invasive bioelectrodes was measured, as shown in Fig. 4. Neuronal activity measurements without bioelectrode stimulation in Fig. 4a show Pt-IPB with significantly increased WDR neuronal activity ($*p < 0.05$) compared to the negligible change from other groups. This suggests that Pt nanoparticles have superior electrocatalytic[44–46] and charge transfer properties,[47–49] and therefore, WDR neuronal activity of Pt-IPB has highly increased upon just bioelectrode insertion, i.e., without bioelectrode stimulation.

Neuronal activity measurements with bioelectrode stimulation in Fig. 4b show that as compared with ICB, the IPB and all x-IPB groups have significantly increased LT and WDR neuronal activity ($*p < 0.05$). In addition, LT neuronal activity in IPB and all
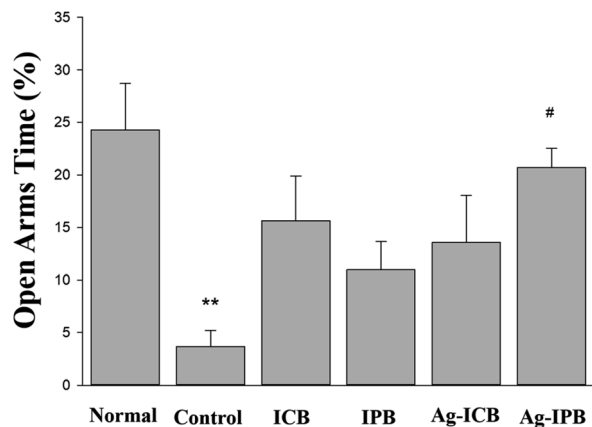
Fig. 5 Comparison of percentages of open arms time compared to the entire time during withdrawal from chronic alcohol treatment in each group.

x-IPB groups was significantly improved than without stimulation, suggesting that higher stimulation through bioelectrode rotation increases the electrical signals *in vivo*. The Ag-IPB group especially demonstrated significantly increased WDR neuronal activity through the bioelectrode stimulation, which is believed to be a result of the high electrical conductivity and charge transfer properties of Ag nanoparticle.[50,51] Also, the increased WDR neuronal response following stimulation show increased action potential intensity, therefore potentially improving synaptic plasticity and the flexibility of neuronal response.[52] This increase is significantly different from the LT neuronal response, which can effectively generate more electrical signals depending on the stimulation. Consequently, the high surface area and noble metal sensitization of all x-IPB groups enhance the electrical coupling with the surrounding tissue/cells, which eventually increased the signal intensity that activated the neurotransmitter receptors.[53–59] Also, the superiority of the noble metal sensitized invasive bioelectrode, identified through neuronal activity measurements, is expected to make a great contribution to the field of neuro research, *e.g.*, neural stimulation,[36] modulation of neuronal behavior,[37] neurotransmitter detection,[38] and intrinsic therapeutic measurements.[39]

By utilizing this higher neuronal activity of noble metal sensitized invasive porous bioelectrodes, we further evaluated the efficacy of bioelectrode treatments in the treatment of chronic alcoholism as measured in an animal model of alcohol withdrawal anxiety as shown in Fig. 5. The EPM test, in which anxiety reduction is directly related to an increase in the time spent in the open arm section of the maze,[57] was used to measure anxiety in both normal and alcohol-treated Sprague-Dawley (SD) rats. Anxiety-states, such as those experienced during alcohol withdrawal, are one of the leading factors for alcohol dependency and relapse.[60] Reduction of anxiety during alcohol withdrawal can therefore significantly reduce the possibility of such relapse and thus serve as a basis for the treatment of chronic alcoholism. As seen in Fig. 5, higher anxiety (lesser time spent in open arms) is measured among the ethanol-induced control group compared to the normal group.

Upon chronic alcohol treatment by invasive bioelectrodes, the time spent in open arms are significantly higher than the control groups which correlate to reduction in anxiety and thus reflects a neuropsychologically-mediated alcohol detoxification.

Among the noble metals, Ag-IPB appears to the most suitable bioelectrode for these studies. It can be observed in Fig. 3a that the Ag-IPB has the lowest charge transfer resistance after an electrodeposition time of 75 s and that this device has a relatively smaller curve radius compared to the other bioelectrodes, implying that electrons flow with minimal resistance due to the low R_{CT}. Another reason is due to its higher WDR neuronal response with bioelectrode stimulation (Fig. 4b), which more effectively generates electrical signals.[52] Moreover, as compared to Pt nanoparticles, Ag nanoparticles are more suitable for biocompatibility, safety, and productivity in the therapeutic field.[61,62] In Fig. 5, Ag-IPB significantly increased the open arms time compared to other groups. Ag-IPB has a larger surface area and a greater number of Ag nanoparticles applied to the surface than IPB and Ag-ICN; thus, both factors could have enhanced the electrical interaction with surrounding tissues/cells, as mentioned earlier.[50–53] In aggregate, we determined that Ag-IPB has the most excellent anxiety mitigation effect as induced by chronic alcoholism-related withdrawal syndromes, as demonstrated in this animal model.

3. Conclusion

In summary, noble metal sensitized invasive porous bioelectrodes demonstrate enhanced electro-physiological neuronal activity, compared to conventional and unsensitized invasive porous bioelectrodes. Also, noble metal sensitized invasive porous bioelectrodes show significantly greater biological activity, with respect to increased LT and WDR neuronal activity. In particular, we found that the Pt-IPB increased WDR neuronal activity even without stimulation. Moreover, the Ag-IPB increased LT and WDR neuronal activity upon stimulation to a greater extent than the other devices, because this system has highest surface area and improved electrochemical properties that enhance the electrical interaction with the surrounding cells and tissues. Furthermore, we have shown in an animal model of alcohol withdrawal triggered anxiety that the Ag-IPB effectively mitigates this anxiety, contributes to detoxification, and thus may play a role in a potential treatment for chronic alcoholism. However, it will involve several issues, such as nanoparticle releases and the complexity of *in vivo* measurements. Nonetheless, these superior results of the noble metal sensitized invasive bioelectrodes suggest the medical utility of surface-modified invasive bioelectrodes. We believe our results will enable new opportunities for improving therapeutic outcomes.

4. Experimental section

4.1. Invasive porous bioelectrodes (IPBs) fabrication

Invasive porous bioelectrodes (IPBs) were fabricated by electrochemical anodization of invasive conventional bioelectrodes (ICBs), as reported previously.[32] The ICBs (stainless steel type

304, 8.0 mm length and 0.18 mm diameter) utilized in this investigation were purchased from Dongbang Acupuncture Inc., Republic of Korea, and were sequentially washed in acetone, ethanol and deionized (DI) water prior to electrochemical anodization. A two-electrode cell was used for anodization employing carbon paper (Carbon and Fuel Cell, CNL, Republic of Korea) as a counter electrode, ICB as a working electrode, and the distance between the two electrodes was 1 cm. The electrolyte consisted of 0.2 wt. % (weight percent) NH_4F (98.0%, American Chemical Society (ACS) reagent, Alfa Aesar, United States) and 2.0 vol. % (volume percent) DI water in ethylene glycol. The anodization was performed at room temperature for 30 minutes with an applied voltage of 20 V; the resulting IPB was then washed consecutively with acetone, ethanol and DI water, followed by drying using a nitrogen gas stream.

4.2. Deposition of noble metal nanoparticles on invasive porous bioelectrodes (x-IPBs)

Silver, gold, or platinum nanoparticles were deposited on the surface of the IPBs by electrodeposition; the bioelectrode are identified as x-IPB, where x = Ag, Au, Pt. Noble metal nanoparticle electrodeposition was carried out in a two-electrode cell, with an IPB used as the working electrode and carbon paper as the counter electrode, and distance between the two electrodes was 1 cm. The electrolyte used for each of the electrodeposition was composed of 0.02 wt. % chemical reagent and 2.0 vol. % DI water in ethylene glycol. The chemical reagents used were $AgNO_3$ (99.0%, American Chemical Society (ACS) reagent, Sigma Aldrich) for Ag-IPB, $NaAuCl_4 \cdot 2H_2O$ (99.0%, Sigma Aldrich) for Au-IPB, and $H_2PtCl_6 \cdot 6H_2O$ (≥37.50% Pt basis, American Chemical Society (ACS) reagent, Sigma Aldrich) for Pt-IPB. In all cases, the electrodeposition voltage was 2.0 V, with varying deposition time, i.e. 45 s, 60 s, 75 s, 90 s, 105 s and 120 s. Based on electrochemical impedance spectroscopy (EIS) an electrodeposition time of 75 s was selected as being optimal, with the bioelectrodes under this condition demonstrating minimum charge transfer resistance. After electrodeposition, the x-IPB were thoroughly washed with hot DI water (70 °C) to remove any loosely attached nanoparticles, and then dried under a nitrogen gas stream. Also, in order to compare the noble metal nanoparticle structures, silver, gold, or platinum nanoparticles were deposited on the surface of the ICBs using the same method.

4.3. Characterization

Surface morphologies were studied using a Field Emission Scanning Electron Microscope (FE-SEM, Hitachi S-4800) operating at 3 kV and 10 μA. Elemental analysis was obtained using Energy Dispersive Spectroscopy (EDS, Brucker Co.). Surface areas were estimated using dye adsorption/desorption; the UV-Vis spectra (550–750 nm) for the methylene blue dye solution desorbed from ICB, IPB and x-IPB was obtained using a Cary series UV-Vis near IR spectrophotometer (UV-Vis spectrophotometer, SHIMADZU UV-2600). Electro-chemical impedance spectra were obtained using a Bio Logic SAS (Model VSP-1158)

three-electrode workstation with platinum (Pt) wire as the counter electrode, Ag/AgCl electrode as the reference electrode, and ICB, IPB and x-IPB as working electrodes. The system was operated using EC Lab software in the frequency range of 100 kHz to 20 Hz with saline solution (0.9 g NaCl in 100 ml DI water) as an electrolyte, purchased from JW-Pharma, Republic of Korea.

4.4. Invasive bioelectrode efficacy measurement

Invasive bioelectrode efficacy was evaluated by using electrophysiology in male Sprague-Dawley (SD) rats. Changes in the spinal dorsal neuronal response activity in response to bioelectrode stimuli were measured using in vivo extracellular recording. The bioelectrodes were manually inserted to 3 mm depth at the receptive field of rat hind paw glabrous skin. As reported previously, bioelectrode stimulation at 3 mm depth showed superior functional effects.[63] After insertion, a probe holder was used to maintain the vertical position of the bioelectrode, with stimulation performed manually with left and right rotation (twisting) of the invasive bioelectrode (rotation per second) for 10 seconds. SD rats were randomly divided into five groups on the basis of invasive bioelectrode as; ICB (n = 21), IPB (n = 10), Ag-IPB (n = 11), Au-IPB (n = 13), and Pt-IPB (n = 11), respectively.

4.5. Animal preparation for neuronal activity measurements

Male SD rats obtained from Harlan Sprague-Dawley (HyoChang Co., South Korea) were housed (2–3 rats in a rat cage, 42W cm × 28L cm × 18D cm) with a light/dark cycle of 12/12 h (temperature 22 ± 3 °C and humidity 55 ± 10%) and fed ad libitum. The animal protocols were reviewed and approved (Protocol#: DHU2015-072) by the Daegu Haany University Animal Care committee and were carried out in accordance with the National Institute of Health (NIH) Guide for the Care and Use of Laboratory Animals. After anesthesia (sodium pentobarbital, i. p., 60 mg kg^{-1}), the low thoracic spinal laminectomy was performed which exposes lumbar 4–5 spinal dorsal horn regions that receive the sensory inputs originating from the hind paw. The spinal vertebral columns were strongly clamped rostrocaudally using stereotaxic apparatus and tracheal and jugular vein cannula were inserted for continuous breathing and a constant level of anesthesia during measurement of spinal dorsal horn neuronal activity. During the in vivo extracellular recording, the rats were maintained at adequate anesthetic condition by continuous sodium pentobarbital infusion (5 mg kg^{-1} h^{-1}, i. v.).

4.6. Neuronal activity measurements

A single-microcarbon filament-filled glass electrode (Carbostar-1 recording carbon microelectrode, Kationic Scentific, Minneapolis, USA) was used for the measurement of in vivo single unit neuronal activity in response to bioelectrode stimulation in the lumbar (L4-5) spinal dorsal horn. Briefly, a glass electrode was inserted into spinal dorsal horn (depth 150–700 μm from dorsal surface) using a micromanipulator (Narishige, MHW-4 One-axis Water Hydraulic Micromanipulator, Narishige, Amityville, NY,

USA), and the single action potential signal was measured in response to bioelectrode stimulation. After insertion into the hind paw receptive field, the bioelectrode was stimulated by twisting (1 Hz, 10 seconds). After isolating a single neuronal activity, the phenotype of neuron was characterized by 5 different intensities of von Frey filaments (VFFs log unit 4.31 (2.04 g), 4.56 (3.31 g), 4.74 (5.50 g), 4.93 (8.32 g) and 5.18 (14.45 g)). Spinal dorsal horn neurons were divided into wide dynamic range (WDR) and low threshold (LT) neurons according to their response patterns to the increasing mechanical stimuli. LT neurons generally showed strong activity to weak intensity stimuli, whereas WDR neurons showed graded response patterns to increasing stimuli intensities. After isolation and confirmation of the neuronal type, the signals were amplified (300 Hz to 10 kHz band pass filter, voltage gain 104; ISO-80, WPI, Sarasota, FL, USA) and fed into the data acquisition unit (CED-1401; Cambridge Electronic Design, UK). The signals were collected and analyzed by Spike2 software (ver. 7.09). Invasive bioelectrode effects on the neuronal response activity and spontaneous activity (without stimulation, 20 s) were measured at both before and after bioelectrode stimulation. Data is presented as mean frequency per second (Hz s^{-1}) and evaluated as % changes. Statistical analysis was conducted using repeated two- or one-way analysis of variance (ANOVA), employing the Tuckey method for multiple comparisons. An alpha level of significance was set at 0.05 for all statistical tests using the SigmaStat program (ver. 3.1).

To avoid differential sensitivity to mechanical stimulation in each rat, paw withdrawal thresholds (PWTs) were measured prior to the electrophysiological experiments, and rats with abnormal ranges of thresholds in normal conditions were removed from the study. PWTs were measured by changes of mean paw withdrawal thresholds to calibrate von Frey filaments (VFFs), beginning with the 4.31 and a series of VFFs was 3.61 (0.45 g), 3.84 (0.74 g), 4.08 (1.26 g), 4.31 (2.04 g), 4.56 (3.31 g), 4.74 (5.50 g), 4.93 (8.32 g) and 5.18 (14.45 g), determined by 50% withdrawal mechanical threshold using the formula:

$$\log(50\% \text{ threshold}) = 10(X_f + k\delta)/10\ 000$$

where, X_f = value of the final von Frey filament (log unit), k = correction factors (taken form calibration table), and δ = mean differences of log units between stimuli; the 18 g pressure of 50% withdrawal threshold measurement (according to up–down method) was selected as the cut-off value.[64]

4.7. Animal preparation for alcohol treatment measurements

Male SD rats (Daehan Animal, Seoul, Korea) weighing approximately 260 g at the start of the experiment were used. Rats were kept in the environment of 12 h light–dark cycle (turn on at 7:00 p.m.), room temperature (22 ± 2 °C), and humidity (60 ± 2%). They were allowed to freely access food and water. After at least 3 days of adaptation, animals were subjected to the experiments. Rats were treated under minimized stress cross over all experiments in compliance with the protocols approved by the

Institutional Animal Care and Use Committee at Daegu Haany University.

4.8. Alcohol treatment measurements

Following 3 days of adaptation period in the animal room, animals of the normal group were treated with saline, and the other groups were treated with ethanol (i.p.; 3 g kg^{-1}; 20% w v^{-1}; Merck KGaA, Darmstadt, Germany) for 21 days. Following the treatments of ethanol or saline for 21 days, rats were given withdrawal for 2 days. Rats were divided into the following 6 groups: (1) ICB, inserted into HT7 with invasive conventional bioelectrode; (2) IPB, inserted into HT7 with invasive porous bioelectrode; (3) Ag-ICB, inserted into HT7 with Ag nanoparticle sensitized invasive conventional bioelectrode; (4) Ag-IPB, inserted into HT7 with Ag nanoparticle sensitized invasive porous bioelectrode; (5) control and (6) normal received the same treatment with other groups without insertion. Each group $n = 8$. After the withdrawal period, invasive bioelectrode treatment was performed for 1 min at bilateral acupoints immediately before the animals were subjected to the elevated plus maze (EPM) test. Invasive bioelectrodes were inserted vertically into a depth of 2–3 mm. Stimulation was produced by bi-directional twisting of the bioelectrode at a frequency of twice per second for a total of 2 s while inserting and withdrawing. Invasive bioelectrode treatment was performed in an awake status under a slight restriction of movement. Daily handling was given for 2–3 min across all experiments to minimize the stress from the movement restriction. HT7 is located on the transverse crease of the wrist of the forepaw, radial to the tendon of the muscle flexor carpi ulnaris.[2,33,65] The anatomical locations of acupoints were determined according to those in animal bioelectrode atlases.[66] The EPM chamber was made of black acrylic and was consisted of four arms (50 cm long × 10 cm wide). Two open arms had high ledges of 0.5 cm and lighting was 1.5 to 2.0 lux. Two closed arms had 40 cm high dark acrylic walls. The chamber was elevated 40 cm from the floor. White noise was maintained constantly as 70 dB during all experiments. First, rats were given 2 h of habituation time under the test condition (lighting and white noise) in the test room. At the test, when rats were placed onto the center platform of the EPM apparatus and the start button was clicked on the computer, time spent in the arms were measured automatically for 5 min by a video tracking system (Ethovision, Netherlands) equipped on the roof and the time spent in each arm calculated by the computer. Each rat was naive to the apparatus, and preferential time in the open arm was interpreted as being inversely related to anxiety levels. The chamber was cleaned with distilled water and was dried after each trial.[67,68] EPM data were analyzed using a one-way ANOVA and post hoc Tukey test. The statistical significance was regarded with a P value less than 0.05.

Ethical statement

All animal experiments were approved by and performed in accordance with the guidelines of the Institutional Animal Care

and Use Committee at the Daegu Haany University (Approval No. DHU2019-019).

Author contribution

Conflicts of interest

There authors declare no competing financial interest.

Acknowledgements

Notes and references

1 R. B. Kelly, *Am. Fam. Physician*, 2009, **80**, 481.
2 W. Jin, M. S. Kim, E. Y. Jang, J. Y. Lee, J. G. Lee, H. Y. Kim, S. S. Yoon, B. H. Lee, S. Chang, J. H. Kim, K. H. Choi, H. Koo, Y. S. Gwak, S. C. Steffensen, Y.-H. Ryu, H. Y. Kim and C. H. Yang, *Addict. Biol.*, 2018, **23**, 165.
3 M. P. Freeman, M. Fava, J. Lake, M. H. Trivedi, K. L. Wisner and D. Mischoulon, *J. Clin. Psychiatr.*, 2010, **71**, 669.
4 B. B. Johansson, E. Haker, M. v. Arbin, M. Britton, G. Långström, A. Terént, D. Ursing and K. Asplund, *Storke*, 2001, **32**, 707.
5 D. Melchart, A. Streng, A. Hoppe, B. Brinkhaus, C. Witt, S. Wagenpfeil, V. Pfaffenrath, M. Hammes, J. Hummelsberger, D. Irnich, W. Weidenhammer, S. N. Willich and K. Linde, *Br. Med. J.*, 2005, **331**, 376.
6 T. M. Cummings and A. R. White, *Arch. Phys. Med. Rehabil.*, 2001, **82**, 986.
7 C. Witt, B. Brinkhaus, S. Jena, K. Linde, A. Streng, S. Wagenpfeil, J. Hummelsberger, H. U. Walther, D. Melchart and S. N. Willich, *Lancet*, 2005, **366**, 136.
8 M. Haake, H.-H. Müller, C. S. Brittinger, H. D. Basler, H. Schäfer, C. Maier, H. G. Endres, H. J. Trampisch and A. Molsberger, *Arch. Intern. Med.*, 2007, **167**, 1892.
9 L. Lao, *J. Altern. Complementary Med.*, 1996, **2**, 23.
10 A. White and E. Ernst, *Rheumatology*, 2004, **43**, 662.
11 L. Lao, *J. Altern. Complementary Med.*, 1996, **2**, 23.

12 H. S. Hwang, E. J. Yang, Y. H. Ryu, M. S. Lee and S.-M. Choi, *J. Acupunct. Meridian Stud.*, 2010, **3**, 89.
13 H. M. Langevin and J. A. Yandow, *Anat. Rec.*, 2002, **269**, 257.
14 B. Zhou, M. Mao, X. Cao, M. Ge, X. Tang, S. Li, D. Lin, L. Yang and J. Liu, *Anal. Chem.*, 2018, **90**, 3826.
15 P. Li, B. Zhou, X. Cao, X. Tang, L. Yang, L. Hu and J. Liu, *Chem. - Eur. J.*, 2017, **23**, 14278.
16 L. Tang, D. Du, F. Yang, Z. Liang, Y. Ning, H. Wang and G.-J. Zhang, *Sci. Rep.*, 2015, **5**, 11627.
17 A. Walling, *J. Am. Acad. Nurse Pract.*, 2006, **18**, 135.
18 H. M. Langevin, D. L. Churchill and M. J. Cipolla, *FASEB J.*, 2001, **15**, 2275.
19 C. H. Yang, B. H. Lee and S. H. Sohn, *Evid. base Compl. Alternative Med.*, 2008, **5**, 257.
20 G. Wang, Q. Gao, J. Li, Y. Tian and J. Hou, *Am. J. Phys. Med. Rehab.*, 2016, **95**, 483.
21 X. Zhang, H.-J. Park and H. Lee, *Integr. Med. Res.*, 2015, **4**, 66.
22 F. Ceccherelli, M. Bordin, G. Gagliardi and M. Caravello, *Acupunct. Electrother. Res.*, 2001, **26**, 229.
23 L.-W. Chou, Y.-L. Hsieh, T.-S. Kuan and C.-Z. Hong, *Biomedicine*, 2014, **4**, 13.
24 X. Niu, Z. Wen, X. Li, W. Zhao, X. Li, Y. Huang, Q. Li, G. Li and W. Sun, *Sens. Actuators, B*, 2018, **255**, 471.
25 L. Tang, Y. Li, H. Xie, Q. Shu, F. Yang, Y.-L. Liu, F. Liang, H. Wang, W. Huang and G.-J. Zhang, *Sci. Rep.*, 2017, **7**, 6446.
26 T. Huang, W. Zhang, S. Jia, Y. Tian, G. Wang, L. Yang, I. Gaischek, L. Wang and G. Litscher, *Evid. base Compl. Alternative Med.*, 2012, **2012**, 157989.
27 T. Huang, X. Huang, W. Zhang, S. Jia, X. Cheng and G. Litscher, *Evid. base Compl. Alternative Med.*, 2013, **2013**, 905852.
28 H. Zhu, *Med. Acupunct.*, 2014, **26**, 264.
29 K. Zhou, J. Fang, X. Wang, Y. Wang, Y. Hong, J. Liu, L. Wang, C. Xue, P. Wang, B. Liu and B. Zhu, *J. Altern. Complementary Med.*, 2011, **17**, 1007.
30 X.-Y. Ynag, G.-X. Shi, Q.-Q. Li, Z.-H. Zhang, Q. Xu and C.-Z. Liu, *Evid. base Compl. Alternative Med.*, 2013, **2013**, 319734.
31 T. Lundeberg, *Acupunct. Med.*, 2013, **31**, 129.
32 S.-I. In, Y. S. Gwak, H. R. Kim, A. Razzaq, K.-S. Lee, H. Y. Kim, S. Chang, B. H. Lee, C. A. Grimes and C. H. Yang, *Sci. Rep.*, 2016, **6**, 34061.
33 B. R. Lee, H.-R. Kim, E.-S. Choi, J.-H. Cho, N.-J. Kim, J.-H. Kim, K.-M. Lee, A. Razzaq, H. Choi, Y. Hwang, C. A. Grimes, B.-H. Lee, E. Kim and S.-I. In, *Sci. Rep.*, 2017, **7**, 12900.
34 S. Sorcar, C. A. Grimes and S.-I. In, *J. Acupunct. Meridian Stud.*, 2018, **11**, 107.
35 K.-W. Kim, S. Hong, H. S. Kim, T. Kim, J. Ahn, H.-S. Song, Y.-K. Kim, J.-Y. Oh, T.-Y. Hwang, H. Lee and S.-I. In, *PloS One*, 2019, **14**, e0226304.
36 B. Si and E. Song, *Chemosensors*, 2018, **6**, 1.
37 C. Paviolo and P. R. Stoddart, *Nanomaterials*, 2017, **7**, 92.
38 E. Colombo, P. Feyen, M. R. Antognazza, G. Lanzani and F. Benfenati, *Front. Neurosci.*, 2016, **10**, 105.

39 R. R. Arvizo, S. Bhattacharyya, R. A. Kudgus, K. Giri, R. Bhattacharya and P. Mukherjee, *Chem. Soc. Rev.*, 2012, **41**, 2943.

40 A. J. Arvizo, B. Casal, E. R. Hizky, I. L. Arbeloa, F. L. Arbeloa, J. Santaren and A. Alvarez, *Clay Miner.*, 1992, **27**, 101.

41 Y. S. Gwak, S. E. Hassler and C. E. Hulsebosch, *Pain*, 2013, **154**, 1699.

42 R. R. Arvizo, S. Bhattacharyya, R. A. Kudgus, K. Giri, R. Bhattacharya and P. Mukherjee, *Chem. Soc. Rev.*, 2012, **41**, 2943.

43 A. A. Minea, *Nanomaterials*, 2019, **9**, 1592.

44 J. K. Nørskov, T. Bligaard, A. Logadottir, J. R. Kitchin, J. G. Chen, S. Pandelov and U. Stimming, *J. Electrochem. Soc.*, 2005, **152**, J23.

45 J. K. Nørskov and C. H. Christensen, *Science*, 2006, **312**, 1322.

46 S. Trasatti, *J. Electroanal. Chem. Interfacial Electrochem.*, 1972, **39**, 16.

47 B. C. Han, C. R. Miranda and G. Ceder, *Phys. Rev. B: Condens. Matter Mater. Phys.*, 2008, **77**, 75410.

48 M. Shao, A. Peles and K. Shoemaker, *Nano Lett.*, 2011, **11**, 3714.

49 T. Reier, M. Oezaslan and P. Strasser, *ACS Catal.*, 2012, **2**, 1765.

50 B. Yang, Z. Yang, R. Wang and Z. Feng, *J. Mater. Chem. A*, 2014, **2**, 785.

51 M. Nycz, K. Arkusz and D. G. Pijanowska, *Nanomaterials*, 2019, **9**, 1072.

52 R. D'Mello and A. H. Dickenson, *Br. J. Anaesth.*, 2008, **101**, 8.

53 M. Shevach, S. Fleischer, A. Shapira and T. Dvir, *Nano Lett.*, 2014, **14**, 5792.

54 P. Polak and O. Shefi, *Nanomed. Nanotechnol. Biol. Med.*, 2015, **11**, 1467.

55 N. A. Kotov, J. O. Winter, I. P. Clements, E. Jan, B. P. Timko, S. Campidelli, S. Pathak, A. Mazzatenta, C. M. Lieber, M. Prato, R. V. Bellamkonda, G. A. Silva, N. W. Shi Kam, F. Patosky and L. Ballerini, *Adv. Mater.*, 2009, **21**, 3970.

56 A. T. Young, N. Cornwell and M. A. Daniele, *Adv. Funct. Mater.*, 2018, **28**, 1700239.

57 S. Pellow, P. Chopin, S. E. File and M. Briley, *J. Neurosci. Methods*, 1985, **14**, 149.

58 D. Nguyen, P. Deng, E. A. Matthews, D.-S. Kim, G. Feng, A. H. Dickenson, Z. C. Xu and Z. D. Luo, *Mol. Pain*, 2009, **5**, 6.

59 Y. Fan, D.-H. Kim, Y. S. Gwak, D. Ahn, Y. Ryu, S. Chang, B. H. Lee, K. B. Bills, S. C. Steffensen, C. H. Yang and H. Y. Kim, *Brain Behav. Immun.*, 2020, DOI: 10.1016/j.bbi.2020.08.016.

60 G. R. Valdez, V. Sabino and G. F. Koob, *Alcohol Clin. Exp. Res.*, 2004, **28**, 865.

61 D. Pedone, M. Moglianetti, E. D. Luca, G. Bardi and P. P. Pompa, *Chem. Soc. Rev.*, 2017, **46**, 4951.

62 Y. Miko, F. Matthew and W. P. Tarl, *WIRES Nanomed. Nanobi.*, 2015, **7**, 428.

63 S. A. Kim, B. H. Lee, J. H. Bae, K. J. Kim, S. C. Steffensen, Y.-H. Ryu, J. W. Leem, C. H. Yang and H. Y. Kim, *PLoS One*, 2013, **8**, e81018.

64 S. R. Chaplan, F. W. Bach, J. W. Pogrel, J. M. Chung and T. L. Yaksh, *J. Neurosci. Methods*, 1994, **53**, 55.

65 S. Lim, *OA Altern. Med.*, 2010, **7**, 167.

66 A. M. Schoen, *Veterinary acupuncture: ancient art to modern medicine*, American Veterinary Publication, Goleta, CA, 1994.

67 S. Chang, Y. Fan, J. H. Shin, Y. Ryu, M. S. Kim, S. C. Steffensen, H. K. Kim, J. M. Kim, B. H. Lee, E. Y. Jang, C. H. Yang and H. Y. Kim, *Mol. Neurobiol.*, 2019, **56**, 7594.

68 D. H. Kim, N. J. Kim, R. J. Zhao, D. H. Kim, C. H. Yang, H. Y. Kim, Y. S. Gwak, E. Y. Jang, J. S. Kim, Y. K. Lee, H. J. Lee, S. C. Lim and B. H. Lee, *Neurosci. Lett.*, 2018, **664**, 38.